Theor Chim Acta (1995) 91: 237–248

Theoretica Chimica Acta

Ab initio molecular dynamics – Applications to the molecular and solid state physics of phosphorus

D. Hohl

Institut für Festkörperforschung, Forschungzentrum Jülich GmbH, D-52425 Jülich, Germany

Received May 25, 1994/Final revision received October 24, 1994/Accepted October 28, 1994

Summary. We review combined molecular dynamics (MD) and density functional (DF) simulations and their applicability in chemistry and physics. This method (also termed *ab initio* MD, "first principles" MD or "Car-Parrinello" method) exhibits characteristic strengths and weaknesses, and we demonstrate both in a set of typical example applications from molecular physics (phosphorus clusters) and soild state physics/chemistry (liquid phosphorus). Dynamical, finite temperature, simulations deriving interatomic forces from state-of-the-art density functional calculations represent a substantial advance over both (i) traditional pointwise total energy and electronic band structure calculations and (ii) classical MD simulations with empirical or semi-empirical forces, and have already yielded qualitatively new insights in several fields.

Key words: Ab initio molecular dynamics – Phosphorus – Clusters – Liquid phoshorus

1 Introduction

The calculation of structures and properties of molecules, solids and liquids has experienced a decade-long steep upwards development with two separate landmark developments:

⇉ *Molecular dynamics* (MD) [1], the numerical solution of the classical (e.g. Newton's) equations of motion (EOM) of an N-particle system with finite difference methods. MD, much like the related Monte Carlo (MC) method, can perform the task of computing macroscopic quantities based on atomistic simulations and providing a direct view of structure and dynamics in the microscopic world of complex systems.
⇉ *Density functional theory*, a variational method originally from solid state physics [2] for the solution of the ground state problem of n electrons interacting with one another and with N nuclei that is now rapidly gaining ground also in the quantum chemistry community [3].

Both fields suffer from a set of characteristic drawbacks when viewed in isolation:

⇉ MD can treat large numbers of particles (up to 10^7) at finite termperatures but relies on an *a priori* qualitative and quantitative knowledge of the interaction

between the particles. Although this approach has provided much important qualitative insight into the structure and dynamics of, e.g. liquids and polymers, it often fails when covalent chemical bonding comes into play and when specific materials properties rather than universal ones are sought.
⇉ Density funcational methods, like other first principles solid state physics and quantum chemistry methods, can treat complex chemical bonds with high precision, and with no input other than the type of atoms in the material. These methods, however, were long confined to point-by-point calculations for a small number of highly symmetric isomers or crystal structures, with small numbers of symmetry-nonequivalent particles (2–30) because of the high computational demand.

In this paper, we review an important development unifying MD (Sect. 2) and DF methodology (Sect. 3) proposed by Car and Parrinello 1985 [4]. We briefly describe the "*ab initio* Molecular Dynamics" method (Sect. 4, detailed reviews can be found in [5–8]), give an account of the computational machinery and demands, and present two representative applications (Sect. 5): (i) Small clusters of phosphorus atoms P_{2-11} and (ii) the molecular-polymeric phase transition in liquid phosphorus.

2 Molecular dynamics

In MD one follows the "trajectory" $\Gamma(t)$ of a system of N particles (atoms, molecules, etc.), i.e. the evolution in time of the particle velocities and positions $\{\dot{\boldsymbol{R}}_I(t)\}$, $\{\boldsymbol{R}_I(t)\}$. $\boldsymbol{R}_I(t)$ denotes the coordinates of particle I in space. Basic statistical theory teaches that quantities $\langle A\rangle_{\text{time}}$ computed as time averages over the trajectories correspond to ensemble averages of physical "observables"

$$\langle A\rangle_{\text{ens}} \equiv \langle A\rangle_{\text{time}} = \lim_{t\to\infty} \frac{1}{t} \int_0^t A(\Gamma(\tilde{t}))\, \mathrm{d}\tilde{t} \approx \frac{1}{\tau} \sum_{\tilde{\tau}=0}^{\tau} A(\Gamma(\tilde{\tau})). \tag{1}$$

Except for a small number of unrealistic model systems the trajectories $\Gamma(t)$ of the colliding particles cannot be calculated analytically, and one has to resort to numerical methods to solve the equations of motion (EOM)

$$\boldsymbol{F}_I(t) = M_I \ddot{\boldsymbol{R}}_I(t) = -\nabla_{\boldsymbol{R}_I} U(\{\boldsymbol{R}_I(t)\}), \tag{2}$$

$\boldsymbol{F}_I(t)$ is the force (vector) acting on particle I with mass M_I at time t and $U(\{\boldsymbol{R}_I(t)\})$ the (scalar) potential energy of the particles at t, i.e. the sum of interaction energies between all particles at this instant. Equation (2) is a system of $3N$ coupled ordinary, nonlinear, 2nd order differential equations, and must be solved iteratively by discretization in the independent time variable t, symbolically $t = 0 \to t + \Delta t \to t + 2\Delta t \to \cdots \to t_{\text{end}}$. Equation (2) is also an initial value problem where one starts from some set of initial conditions $\{\dot{\boldsymbol{R}}_I(t=0)\}$, $\{\boldsymbol{R}_I(t=0)\}$. The most obvious algorithm to use is also the most widely used, the so-called (third-order) Verlet algorithm

$$R(t+\Delta t) = 2R(t) - R(t-\Delta t) + \frac{\Delta t^2}{M} F(t) + O(\Delta t^4). \tag{3}$$

It becomes clear immediately that even with the largest computing resources one needs to confine oneself to modeling a relatively modest number of interacting

particles over a finite period of time t_{end}. Most MD simulations proceed by filling microscopically small boxes ("MD unit cells") with anywhere from 50 to 10^7 particles and following their motion for 10^3–10^7 time steps Δt. These are still minute periods of "real" time (picosecond to nanosecond range), and one basic difficulty of MD simulations is that even on the fastest available computers physics happens in extreme slow motion ($\sim 10^{15-17}$ times slower than reality).

It is somewhat less obvious that the feasibility of the calculation hinges on the ease with which the interaction energy $U(\{\boldsymbol{R}_I(t)\})$ can be computed since this has to be done in every step of the calculation. For that reason, simple pairwise additive short-range interactions of the type

$$U(\{\boldsymbol{R}_I\}) = \sum_{I<J} u(|\boldsymbol{R}_I - \boldsymbol{R}_J|) \tag{4}$$

are most widely used. This type of potential is a good representation for a few interesting systems (e.g. interacting rare-gas atoms) but generally fails when covalent chemical bonds play an important role. The basic reason is that chemical interactions are *not* pairwise additive but are instead governed by the complex electronic structure of the participating atoms. All attempts to model the – fundamentally quantum mechanical – chemical many-body forces between atoms with parametrized models for $U(\{\boldsymbol{R}_I\})$ have so far been blessed with little success. For lack of knowledge, one has to solve – in principle – the full quantum mechanical Schrödinger equation

$$\mathscr{H}\Psi(\{\boldsymbol{R}_I(t)\}, \{\boldsymbol{r}_i\}) = U(\{\boldsymbol{R}_I(t)\})\,\Psi(\{\boldsymbol{R}_I(t)\}, \{\boldsymbol{r}_i\}) \tag{5}$$

with n electrons i in space positions $\boldsymbol{r}_1 \ldots \boldsymbol{r}_i \ldots \boldsymbol{r}_n$. $\mathscr{H}$ is the total quantum-mechanical Hamiltonian operator. Incorporating those additional electronic degrees of freedom increases the computational demand vastly, and we will have to approximate the full Schrödinger equation and simplify the solution.

3 Density functional theory

The density functional formalism [2] shows that a knowledge of the electron density, $n(\boldsymbol{r})$, is sufficient to determine the total energy and other ground state properties of a system of electrons in a potential field, $V_{ext}(\boldsymbol{r})$. In the absence of other fields this is the Coulomb field $V_{ext}(\boldsymbol{r}, \{\boldsymbol{R}_I\})$ of the N nuclei at $\{\boldsymbol{R}_I\}$. The ground state energy, E_{gs}, can be found by minimizing the relationship between energy and density, $E[n]$, and this minimum is found for the ground state density, n_{gs}. It is convenient to write the density functional total energy

$$U_{DFT} = E[n] = T_0[n] + \int d\boldsymbol{r}\, n(\boldsymbol{r})(V_{ext}(\boldsymbol{r}) + \tfrac{1}{2}\Phi(\boldsymbol{r})) + E_{xc}[n] + E_{ion-ion}, \tag{6}$$

where T_0 is the kinetic energy which a system with density n would have in the absence of electron–electron interactions, $\Phi(\boldsymbol{r})$ is the classical Coulomb potential for electrons, and E_{xc} is the exchange-correlation energy. We adopt the widely used LSD approximation $E_{xc}^{LSD} = \int d\boldsymbol{r}\, n(\boldsymbol{r})\, \varepsilon_{xc}[n(\boldsymbol{r})]$, and for the sake of completeness we already added the internuclear repulsion term $E_{ion-ion}(\{\boldsymbol{R}_I\})$.

For a given set of atomic coordinates $\{\boldsymbol{R}_I\}$, $E_{ion-ion}$ is constant and the minimization of $E[n]$ in Eq. (6) is usually performed by solving the Kohn–Sham

equations with electronic Hamiltonian $\mathscr{H}_{el}$

$$(-\tfrac{1}{2}\nabla^2 + V_{ext}(r) + \Phi(r) + V_{xc}(r))\,\psi_i(r) = \varepsilon_i \psi_i(r) \tag{7}$$

The density is constructed from the eigenfunctions of this equation, $n(r) = \sum_i |\psi_i(r)|^2$, with i running over all occupied states.

The one-electron wavefunctions ψ_i are usually expanded in a set of M basis functions $\phi_m(r)$, and the set of partial differential equations (7) becomes a matrix eigenvalue problem with eigenvalues ε_i and eigenvectors c_i (vector length M)

$$\psi_i(r) = \sum_{m=1}^{M} c_{i,m}\,\phi_m(r), \tag{8}$$

$$\sum_m h_{km}\,c_{j,m} = \varepsilon_j\,c_{j,k}, \tag{9}$$

Computationally, the solution of the eigenvalue problem (9) can become very demanding: (i) It is a "pseudo"-eigenvalue problem (the matrix elements $h_{km} = \langle\phi_k(r)|\mathscr{H}_{el}|\phi_m(r)\rangle$ depend on the eigenvectors because the potential in Eq. (7) does) requiring iterative solution to self-consistency. (ii) The dimension of the matrix depends on how well the basis functions $\phi_m(r)$ can represent the distribution of electrons in the substance under investigation. Unfortunately, spatially well-localized "chemical" basis functions (e.g. orbitals of the Slater type) often lead to *small* matrix dimension $M = 100$–1000 but an awkward evaluation of the integrals h_{km}. Functional forms for the $\phi_m(r)$ that offer easy evaluation of the matrix elements tend to require *very large* $M = 10^3$–10^6.

4 Density functional theory and molecular dynamics

The conception of a unified MD–DFT procedure by Car and Parrinello [4] marks one of the most important developments in computational electronic structure theory in decades. One very important ingredient of the MD–DF method is the use of a large ($M = 10^3$–10^6) plane wave basis set for the one-electron eigenfunctions (Eq. (10)) in conjunction with pseudo-potentials for the electron–ion interaction, iterative matrix eigenvalue algorithms, and the realization that FFT methods can be used to perform the necessary convolutions in reciprocal space as multiplications in real space [6, 9].

$$\psi_j(r) = \sum_{m=1}^{M} c_{j\boldsymbol{G}_m} \exp(\mathrm{i}\,\boldsymbol{G}_m r). \tag{10}$$

In MD simulations it is crucial that all degrees of freedom move with EOM that are mutually compatible and conserve the sum of all kinetic and potential energy terms. Within the MD–DF scheme this leads to two coupled sets of EOM for the electronic wavefunctions $\psi_i(t)$ and atomic positions $\boldsymbol{R}_I(t)$

$$\mu\ddot{\psi}_i(r, t) = -\frac{\delta U_{DFT}}{\delta\psi_i^*(r, t)} + \sum_k \Lambda_{ik}(t)\,\psi_k(r, t), \tag{11}$$

$$M_I\ddot{\boldsymbol{R}}_I = -\nabla_{R_I} U_{DFT}(\{\boldsymbol{R}_I(t)\}). \tag{12}$$

These EOM are identical to those in Eq. (2) except that the electronic wavefunctions evolve in time together with the atomic positions, and that now

the first-principles DFT expression U_{DFT} appears as the potential energy of the particles. The ψ_i get fictitious "masses" μ and need to be orthogonalized in every time step with the Langrange multiplier method (Λ_{ik}, second term in Eq. (11)). The same differential equation solvers can be used as in classical MD simulations (see Sect. 2).

5 Applications

5.1 Nanoscale phosphorus clusters

At the boundary between chemistry and physics, microclusters represent a challenge to atomistic modeling. With the discovery of carbon fullerenes, the theoretical interest in these systems extended beyond quantum chemistry into the field of materials science. As can be expected on the basis of simple considerations, the cluster size plays a nontrivial role in determing their properties. With increasing number of atoms N, chemical, optical, dynamical and magnetic properties change in a nonmonotonic way, and only slowly approach those of bulk systems. First-principles electronic structure methods have been particularly useful to describe this evolution, and, for a large class of elements (mainly semiconductors and simple metals), they provide the only reliable model.

We have concentrated on semiconductor clusters in our own work and we will discuss the results for phosphorus clusters P_N representative for other applications. Bulk phosphorus displays a great structural variability characterized by a whole spectrum of chemical and physical properties. Already clusters with only a few atoms present a very large number of isomers, and finding the most stable points of the energy function $U(\{\boldsymbol{R}_I(t)\})$ is a challenging optimization task. Simulated annealing, a method borrowed from statistical theory, can be used here very efficiently in conjunction with the MD–DF method. Studies for P_N clusters with $N = 2$–11 show many unexpected features [9]. They provide valuable information on different subjects, like reactivity, nucleation, and the relation between different solid phases. Figure 1 shows examples of how complicated the cluster geometries can become.

P_N clusters have been identified mass-spectrometrically (MS) with up to $N = 7000$ [10]. The tetrahedral P_4 molecule dominates these spectra, and it is the predominant species in phosphorus vapor. It is also the building block of crystalline white phosphorus and the liquid at low temperatures (see Refs. [11–13] and Sect. 5.2). The stability of P_4 is somewhat surprising since, with an atomic valence electronic configuration of s^2p^3, one would expect a purely p-bonded structure with three neighbors and all bond angles identical 90° to be the natural "island of stability". A P_8 cube would be the perfect realization of this concept, but instead P_8 has never been identified except as minor component in the MS with unknown structure. Although our simulated annealing studies [9] could not provide a clear answer *why* tetrahedral P_4 is so stable, they have exposed the comparison with cubic P_8 as inappropriate: The cube is – by far (1.7 eV) – not the most stable structure of the eight-atom cluster. Instead, it decays over a small energetic barrier into a cradle-like structure (Fig. 1) that, like tetrahedral P_4, possesses 60° angles. Our findings were subsequently confirmed by more traditional quantum chemical calculations [14, 15] and are chemically plausible because the same curious structural P_8 element occurs in crystalline monoclinic "violet" phosphorus [16]. The P_8 cradle structure is slightly *more* stable than two

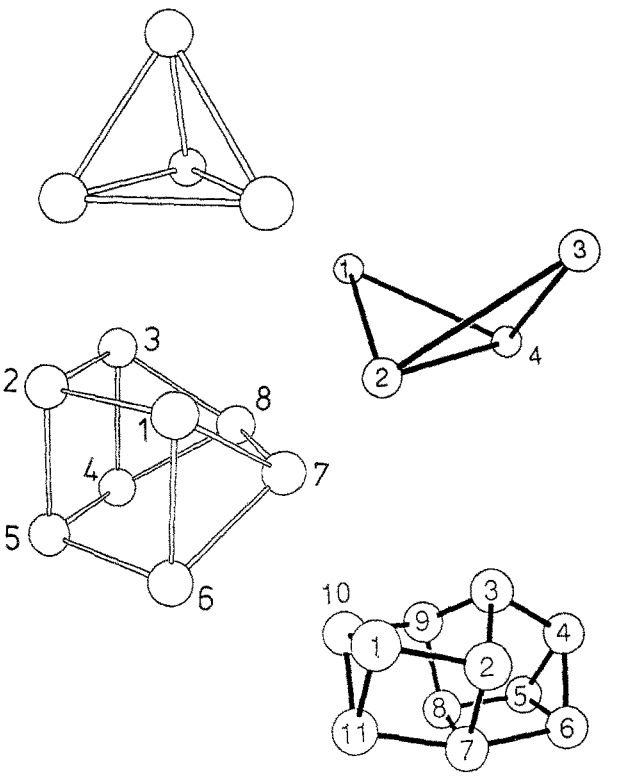

Fig. 1. Structure of two P_4 isomers ("roof" and tetrahedron) and of the most stable geometries of P_8 and P_{11}

tetrahedra in the LDA [9], a puzzling point [14] that was subsequently shown to be an artefact of this particular approximation to electron exchange and correlation and that can be remedied with the inclusion of gradient corrections [17].

Another advantage of cluster calculations like ours with MD–DF is that the computational effort is relatively modest (and scaling only like $N \log N$ for a given size of the periodic box), and that a complete series of cluster sizes N can be investigated to identify "growth patterns". For $P_{3,4}$ the structural basis is an equilateral triangle, for P_{5-7} it is a low-lying excited state of P_4 (the "roof structure, Fig. 1) to which one, two and three atoms, respectively, get attached. At $N = 8$, the growth scheme changes again, and P_{9-11} can best be described as 1–3 atoms attached to the most stable isomer of P_8 [9].

Structural analogies with the isoelectronic hydrocarbon compounds $(CH)_N$ exist (e.g. tetrahedrane, prismane/benzvalene, cubane/cuneane), but the energetic ordering of the isomers can be different. Although no definitive statement can be made concerning $(CH)_8$, all evidence suggests that cubane, like cubic P_8, is less stable than the corresponding cradle structure (cuneane).

All low-energy isomers were calculated with the same general procedure: First we obtain the electronic ground state for some initial "guess" geometry (e.g. a cube of eight P atoms), then the cluster is heated to temperatures in the range $\sim$ 500–10000 K while the trajectory is being visually monitored, and then the "liquid" cluster cooled to temperatures where no structural transformations occur any more (usually near 300 K). Since such a simulated annealing strategy is not guaranteed to locate *the* most stable geometry, the procedure is repeated a few

times starting from different initial structures. It is extremely important in systems with many local minima in the energy surface like P_N to use an approach such as MD that can surmount energy barriers between different minima to obtain a qualitatively correct picture of the system. "Chemical intuition" and pointwise zero-temperature calculations have failed to conceive structures anywhere near the correct one for, e.g. P_6 and P_8.

5.2 Polymerizing liquid molecular phosphorus

We have also performed simulations of liquid phases of phosphorus [18]. If molecular white P is heated above its melting point (315 K), the resulting liquid also comprises tetrahedral P_4 molecules with bond length 2.210 Å [12]. In spite of the compact, almost spherical shape of P_4, neutron diffraction studies of *l-P* show [12] that spatial correlations between the molecules extend farther ($\sim$ 20 Å) than in any other known liquid. Liquid phosphorus turns red if heated above 473 K (boiling point is 553 K) and red amorphous phosphorus (*a-P*) precipitates if the reaction is allowed to proceed. Most industrial processes for converting the poisonous and combustible white P to the more stable *a-P* operate in the vicinity of 500–600 K and require several days for completion. Little is known about the mechanism of this reaction, and experimental studies for its characterization seem to be missing.

The polymeric red *a-P* forms with high molecular weights also contain predominantly threefold coordinated atoms [16]. The average values of the bond lengths and angles are 2.24 Å and 103°, respectively, and red P melts (under pressure) at $\sim$ 875 K to form an almost colorless liquid similar in appearance to molten white P [11]. It is not likely that these two liquids are indeed *identical* [11] and molecular and polymeric components might coexist. Phosphorus differs from its neighbor arsenic in that the molecular $\rightarrow$ polymeric transition occurs in the melt. In As, the polymerization occurs in the solid phase at temperatures of less than 78 K. The driving force behind the transition is in both cases the higher thermodynamic stability of polymeric network strutures over molecular forms that is well known from crystalline modifications [11, 13].

In our study (see also Ref. [18]), we seek to analyze the structures of the molecular and polymeric forms, identify the nature of the medium and long-range order in the molecular liquid, and identify the crucial steps in the polymerization mechanism. While traditional methods of quantum chemistry lead to reliable energies, they are restricted to relatively few atoms and neglect the effects of neighboring ("solvent") molecules, and of nonzero temperature, i.e. the fact that chemical reactions are driven by free energy, not enthalpy alone. These restrictions do not apply to the MD–DF method we use, although its limitations must not be overlooked.

As in our previous work on *a-P* [16], we use a constant-volume cell with lattice constant 27.11 a.u. We therefore expect a good description of local order up to interatomic distances of about 13.5 a.u., i.e. a central tetrahedron in white P together with a complete shell of neighboring molecules. The density was adjusted to that of white P at its melting point ($\rho = 1.81\ \mathrm{g\,cm^{-3}}$) by filling the available volume with 104 P atoms, initially in the form of 26 P_4 tetrahedra. The initial geometry was then heated to a temperature just below where a breakup of the tetrahedra became observable on the time scale of our simulations ($\sim$ 3000 K) to destroy any memory of the initial geometry of the tetrahedra, and then cooled to and equilibrated at $T = 500$ K. A subsequent MD run (5000 steps, $\Delta t = 9$ a.u. in all calculations)

corresponding to a microcanonical ensemble provided the basis for the structural analysis of the molecular liquid. Performing the simulation well above the melting point allows us to accumulate better statistics for all quantities sought because phosphorus is very viscous at the melting point. To verify that the sample is in a diffusive liquid state, we have computed the diffusion coefficient D to be $\sim 5 \times 10^{-4}\,\mathrm{cm^2\,s^{-1}}$. This is within the range of typical liquids.

The only experimental structure study of liquid molecular phosphorus we can compare with are neutron scattering data near the melting point [12]. In Fig. 2 (top) we show the radial distribution functions derived from both our simulations and the scattering data side by side. The agreement is very good up to interatomic distances of about 11 a.u. considering that (i) the temperatures between theoretical and experimental data differ by about 200 K and (ii) no parameter fitting is involved in our computational procedure. The most likely first neighbor distance (i.e. the interatomic separation within the tetrahedral molecules) is slightly larger in our simulations (4.26 a.u.) than in the experimental data (4.18 a.u.), a known effect of the pseudo-potential approximation we use ("s-nonlocality") [16]. The first-neighbor shell defined by the location of the first minimum in $J(r)$ at 5.0 a.u. contains 3.0 atoms, reflecting intact tetrahedra with a small proportion of collision induced 4-fold coordinated defect atoms ($\sim$ 2%; see text below). The overall shape of the $J(r)$ function with a sharp first peak of high intensity dominating over a broader, low-intensity, second neighbor region ($\sim$ 5–9 a.u.) is very well reproduced. The third peak near 10.5 a.u. lies at shorter distances than indicated by the experimental data, but the cell boundary is approached and finite-size effects start to play a role. The closest distance of approach of atoms in *different* molecules in our simulation at 500 K is only $\sim$ 5.2 a.u., substantially less than the sum of two phosphorus van-der-Waals radii (7.2 a.u. [11]), and this "soft core" behavior of the tetrahedra is a crucial element in the polymerization process (see below).

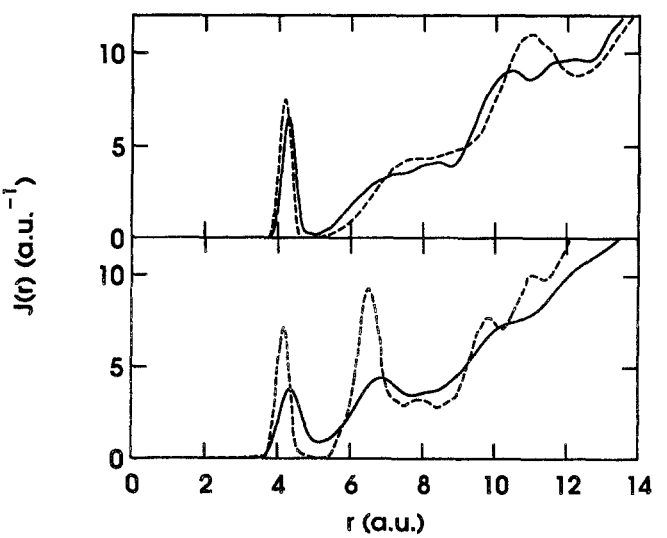

Fig. 2. Radial distribution functions $J(r) = 4\pi r^2 \rho(r)$ in molecular liquid phosphorus (top, solid line: simulation, dashed line: exp.), in the polymeric liquid (bottom, solid line: simulation), and in amorphous phosphorus (bottom, dashed line: exp.) in comparison

Scattering experiments offer little information about the *nature* of intermediate and long-range order. In molecular liquid *P* we define the former as ordering phenomena involving neighboring molecules and the latter as those extending beyond one shell of neighboring molecules and therefore inaccessible in our current simulations of *l-P*. An analysis of the intermediate range order alone, however, has yielded useful insights into what might be the basis of the long-distance correlations in this liquid:

Integrating $J(r)$ (Fig. 2) shows that the second neighbor peak reaching from 5.0 to 8.8 a.u. contains 10 atoms, and the third peak extending from 8.8 to 12.7 a.u. another $\sim$ 32 atoms. This approximate 1 : 3 ratio is compatible with a model [12] where one atom is positioned in the cavity formed by three atoms from other molecules. This model was originally proposed for other liquids of tetrahedral molecules like CCl_4. Analysing, in addition, more complex distribution functions of interatomic distances between neighboring molecules [18] we were able to identify a curious "face-to-face" orientational ordering as the preferred alignment of tetrahedra in near contact (see Fig. 3). Substantial distortions from this alignment are locally possible due to rotational motions of the molecules relative to each other at finite temperature, but radically different orientations like "tip-to-tip" or "tip-to-face" are clearly disadvantageous. At 500 K, we were unable to determine a preference of "staggered" over "eclipsed" configurations of the face-to-face alignment, and that puts an upper bound on the rotational energy barrier. Clearly, the picture of P_4 as a nearly spherical object is inappropriate, and substantial chemical interactions act between neighboring molecules in the liquid.

Modeling the polymerization of white *P* to liquid red *P* is an ambitious endeavor because the reaction is a very slow process requiring typically several days at temperatures between 500 and 600 K. The time scales that are accessible to MD simulations are orders of magnitude shorter, and we have used temperatures much higher than under experimental conditions to accelerate the process. That, in turn, can change the reaction pathways accessible to the system, and the details of

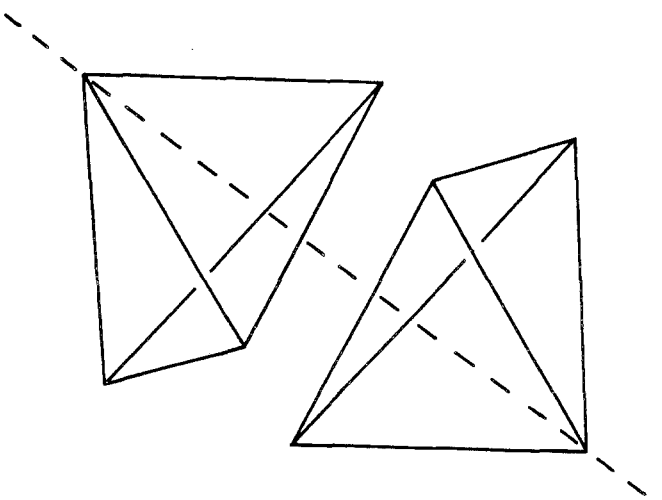

Fig. 3. Schematic drawing of the preferred relative orientation of two neighboring P_4 molecules in molecular *l-P* ("face-to-face")

the mechanism observed [18] must be interpreted with some caution. We still expect that the main features of the polymerization process in phosphorus will be described much more faithfully than parametrized interatomic potentials could do.

Obviously, in the course of the reaction, the individual molecules have to break up and then recombine to form a 3D-network structure similar to that of the amorphous substance [16]. In our simulation the disintegration of P_4 molecules sets in at $T \sim 3000$ K, and no tetrahedron remains intact after 3300 time steps at 3500 K. The mechanism for the breakup is clearly thermally induced collisions between the tetrahedra. Increasing the temperature in a few 1000 timesteps continuously to this point increases primarily the number of 4-fold coordination defects: The molecules bounce into each other but the kinetic energy is not high enough to break them up on the time scale of our observation; 4-fold defects are locally stable [16], but their formation proceeds over an energy barrier. Once this energy barrier can be overcome sufficiently often (i.e. here beyond 3000 K) chemical bonds form between different molecules. 4-fold defects, however, are apparently destabilizing the tetrahedral molecules. We observe rapid structural deformations from the tetrahedral to the "roof" isomer (Fig. 1) in those tetrahedra that contain a fourfold defect, a process breaking one bond in the molecules much in the fashion proposed by Pauling and Simonetta [19] and generating a large proportion of 2-fold coordinated atoms.

With a sufficient number of reactive twofold coordination defects the sample will polymerize rapidly and isotropically at all temperatures between 3500 and

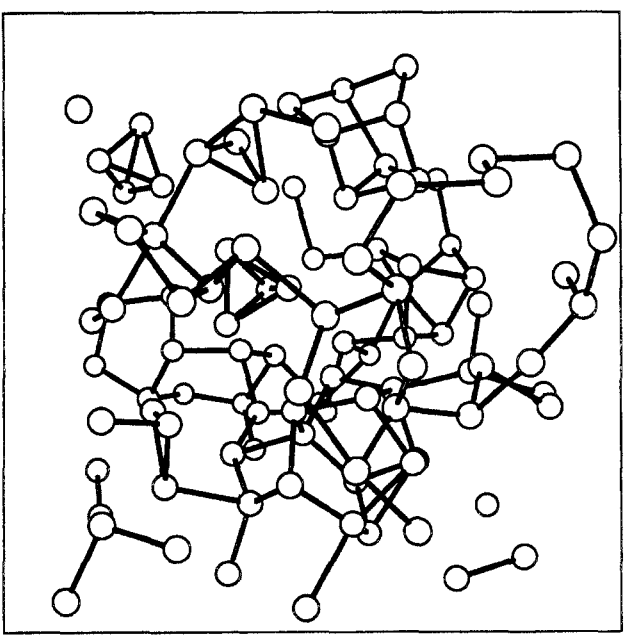

Fig. 4. Snapshot of a typical structure for polymeric liquid phosphorus at $T = 1500$ K. Atoms less than 5.0 a.u. apart are connected by sticks symbolizing bonds. Bonds reaching into the neighboring unit cells are not shown so that atoms near the cell boundaries (edges of the figure) appear artificially undercoordinated

1500 K according to a variety of tests we have performed [18]. Continuing after 3300 steps at 3500 K with 27000 time steps at 1500 K (6 ps) the liquid becomes almost entirely polymeric in nature (two tetrahedra reform). A snapshot of a typical configuration (Fig. 4) shows that the final disordered structure is reminiscent ofthat of *a-P* [16]. One can distinguish interlinked clusters of atoms with shapes resembling those of stable P_N clusters in vacuum, the basic structural model we have developed for *a-P* [16].

An analysis of distribution functions with which we had characterized *a-P* shows close similarity between polymeric *l*-P and *a*-P as well [18]. One example is the radial distribution function $J(r)$. Although we are unaware of any scattering experiments on the polymeric liquid, a comparison between our data for this liquid and experimental data for *a-P* will be illuminating until such experimental data become available. Naturally, the peaks in the liquid are much broader than in the amorphous substance at room temperature (Fig. 2, bottom). The most characteristic differences between the molecular and polymeric substances (Fig. 2, top and bottom, respectively) are the substantial increase in the intensity of the second peak relative to the first, and the shift of its center of mass to lower r. Both are well reproduced by our simulation and we are confident that polymeric liquid phosphorus is indeed structurally very closely related to amorphous phosphorus.

6 Conclusions

The scheme just described provides a powerful and reliable framework to simulate a large class of systems. It can be efficiently applied to locate the optimal structures of small molecular clusters (P_{2-11}) where a method that can overcome local minima in complex energy surfaces is essential to obtain *qualitatively* the correct results. The scheme is quite general conceptually, and it can also describe complex ordering phenomena and phase transitions in chemically bonded liquids and disordered solids. As an example of the latter, we have presented a study of liquid phosphorus in its molecular and polymeric states, and the mechanisms likely involved in their thermal transformation. The most likely pathway involves an opening motion of the P_4 tetrahedra first proposed 40 years ago by Pauling and Simonetta [19]. In studies like this one, the inclusion of finite temperature and the "solvent" are very important and cluster calculations based on single molecules in vacuum at zero temperature are not likely to capture the essential processes.

Limitations remain on the size of the systems we can study (100–400 atoms), on the length of the simulation (ps range), and several chemical elements (most notably transition metals and the elements in the first two rows of the periodic table) are still problematic. These limitations, however, are not fundamental but computational in nature. Algorithm and method development on one side (e.g. new pseudopotentials, basis sets with chemically motivated functional forms [20], linearly scaling methods [21]) and – to a lesser extent – the maturing massively parallel supercomputer technology on the other will advance the field rapidly. The ultimate goal is the capability to perform dynamical calculations for up to 1000 atoms of *any* element in the periodic table.

Acknowledgements. The example applications mentioned here were performed in collaboration with R.O. Jones. I thank P. Ballone for helpful suggestions on an earlier version of this manuscript.

References

1. Alden BJ, Wainwright TE (1957) J Chem Phys 27: 1208
2. Hohenberg P, Kohn W (1964) Phys Rev 136:B864; Kohn W, Sham LJ (1965) Phys Rev 140:A1133
3. Johnson BG, Gill PMW, Pople JA (1992) J Chem Phys 97:7846
4. Car R, Parrinello M (1985) Phys Rev Lett 55:2471
5. Remler DK, Madden PA (1990) Mol Phys 70:921
6. Pastore G, Smargiassi E, Buda F (1991) Phys Rev A 44:6334
7. Oguchi T, Sasaki T (1991) Prog Theor Phys (Suppl) 103:93
8. Payne MC, Teter MP, Allan DC, Arias TA, Joannopoulos JD (1992) Rev Mod Phys 64:1045
9. Jones RO, Hohl D (1990) J Chem Phys 92:6710; Jones RO, Seifert G (1992) J Chem Phys 96:7564
10. Martin TP (1986) Z Phys D 3:211; the MS studies have now been extended to $N \sim 7000$ (Martin TP, Näher U, private communication).
11. Gmelins Handbuch der Anorganischen Chemie, 8. Auflage. Phosphor, Teil B (1964) Handtke G, Bohne-Neuber A, Kirchstein G, Kotowski A, Seuferling F (eds) Chemie, Weinheim/Bergstr.
12. Clarke JH, Dore JC, Granada JR, Reed J, Walford G (1981) Mol Phys 42:861; Granada JR, Dore JC (1982) Mol Phys 46:757
13. Corbridge DEC, Phosphorus. An Outline of its Chemistry, Biochemistry and Technology (Elsevier, Amsterdam, 1985). See Fig. 2.3 for the different forms of elemental phosphorus and pathways for their interconversion.
14. Häser M, Schneider U, Ahlrichs R (1992) J Am Chem Soc 114:9551
15. Janoschek R (1992) Chem Ber 125:2687
16. Hohl D, Jones RO (1992) Phys Rev B 45:8995
17. Ballone P, Jones RO (1994) J Chem Phys 100:4941
18. Hohl D, Jones RO (1994) Phys Rev B 50:17047
19. Pauling L, Simonetta M (1952) J Chem Phys 20:29
20. Harris J, Hohl D (1990) J Phys:Condens Matter 2:5161; Lin Z, Harris J (1993) J Phys:Condens Matter. 5:1055
21. Galli G, Parrinello M (1992) Phys Rev Lett 69:3547; Mauri F, Galli G (1994) Phys Rev B 50:4316; Ordejòn P, Drabold DA, Martin RM, Grumbach M (1993) Phys Rev B 48:14646